

Scaling Qubit Mapping and Routing With Position Graph Abstraction and Memoization

Brent Russon*, Bao G. Bach*[†], Ed Younis[‡], Ilya Safro^{†§}

*Quantum Science and Engineering, University of Delaware, Newark, DE, USA

[†]Computer and Information Sciences, University of Delaware, Newark, DE, USA

[‡]Computational Research Division, Lawrence Berkeley National Laboratory, Berkeley, CA, USA

[§]Physics and Astronomy, University of Delaware, Newark, DE, USA

{bhrusson@udel.edu, baobach@udel.edu, edyounis@lbl.gov, isafro@udel.edu}

Abstract—Scalable qubit mapping and routing remain major bottlenecks in quantum compilation, especially for Trapped-Ion Quantum Charge-Coupled device (TI-QCCD) architectures, where qubit interactions require physically shuttling ions under strict movement, congestion, and trap-capacity constraints. We present a compilation framework built around the position graph abstraction, a unified representation of executable locations, movement paths, and routing constraints that enables heuristic mappers to operate directly on shuttling-based hardware. Using this abstraction, we accelerate the SWAP-based Bidirectional heuristic search (SABRE) by implementing relative move scoring, which caches repeated heuristic move evaluations that arise during search, and memoized congestion resolution, which speeds up the resolution of repeated congestion. This optimization removes redundant computation without changing routing/shuttling decisions, improving the scalability of SABRE-based methods on TI-QCCD systems. Our results show that combining an architecture-aware abstraction with memoized heuristic evaluation yields a practical and effective path toward scalable qubit mapping and routing across heterogeneous quantum architectures. **Reproducibility:** the source code and data are available at [link will be available here upon acceptance]

Index Terms—Quantum Compilation, Superconducting system, Trapped-ion system, Quantum Charge-Coupled Device, Qubit Mapping, Qubit Routing, SABRE, Position Graph

I. INTRODUCTION

Qudit mapping and routing are central bottlenecks in quantum compilation because hardware constraints often prevent logical two-qudit interactions from being executed directly [1], [2]. This challenge is especially important for superconducting architectures and shuttling systems such as trapped-ion quantum charge-coupled device (TI-QCCD) architectures. In superconducting systems, physical qudits can be moved using SWAP operations along a given configuration [3]. In contrast, TI-QCCD requires physically shuttling ions through segments and junctions while respecting movement legality, trap-capacity limits, and congestion constraints [4]. As a result, routing overhead can dominate execution time and strongly affect scalability.

Existing practical mapping methods are largely built around abstractions such as Coupling Graphs, which are well matched to SWAP-based routing on superconducting devices. However, architecture with qudit shuttling [5]–[7], such as TI-QCCD, requires reasoning not only about which qudits should interact, but also about where ions can legally move, which

intermediate positions are occupied, and whether a candidate path is blocked. These constraints make standard connectivity-only abstractions insufficient for expressing the shuttling-based routing. Our prior work addressed this challenge by introducing the *Position Graph* abstraction [8], a hardware-aware representation that captures executable locations, movement paths, and routing constraints within a unified graph model. Built on top of this abstraction, the SHAW and SHAPER [8] compilers showed that heuristic search methods inspired by superconducting-qudit mapping can be adapted to shuttling-based trapped-ion compilation. Although this abstraction is expressive enough to capture the complex TI-QCCD hardware constraints, the initial implementation [8] suffers from scalability issues where it can take a day to shuttle a 128-qudit circuit on a 180-ion space device.

This paper takes the next step toward the practical deployment of the Position Graph abstraction, which substantially improves the scalability, enabling large-scale shuttling with both Superconducting and TI-QCCD architectures. We demonstrate that this richer abstraction does not incur meaningful overhead compared to previous methods, and highlight performance improvements to BQSkat’s SABRE [9], [10] and SHAW algorithms by using cached results of architectural information modeled by the Position Graph. These include finding all-pairs shortest paths, their distance matrix, and an executable subgraph. While the Position Graph enables architecture-aware routing, heuristic search over QCCD states can still incur substantial overhead because the same local blockage and congestion situations are evaluated repeatedly during routing. To reduce this overhead, we introduce *LightSHAW*, a cached variant of SHAW’s congestion-resolution procedure. *LightSHAW* reuses architecture-dependent information such as movement paths and local clearing regions, and it avoids recomputing local congestion scores when the same occupied local configuration recurs during recursive blockage clearing. These caches reduce repeated graph traversal and local occupancy scanning while preserving SHAW’s routing decisions.

In addition to improving SHAW, we evaluate the runtime cost of using the Position Graph abstraction in a standard superconducting routing setting. A concern with richer architectural models is that they may impose unnecessary overhead when the target device is well described by a traditional Cou-

pling Graph. To test this directly, we instantiate LightSABRE using both a conventional Coupling Graph backend and a Position Graph backend. The two implementations perform the same routing decisions and produce identical compiled circuits, allowing the comparison to isolate the cost of the abstraction itself. Our results show that the Position Graph can match the runtime of the Coupling Graph while retaining the ability to represent richer hardware structure when needed. This suggests the practicality of the Position Graph, maintaining runtime while potentially serving as a unification for different types of architectures (we already showed for SWAP-based and shuttling-based architectures).

In summary, this paper makes the following contributions:

- 1) We identify and remove redundant computations in SHAW by caching shortest MOVE paths, travel-time distances, and blockage-related path information used repeatedly during routing.
- 2) We introduce LightSHAW, a cached variant of SHAW that memoizes local congestion geometry and occupancy-sensitive congestion scores, reducing repeated work during recursive blockage resolution while preserving the routing behavior of the original algorithm.
- 3) We demonstrate that the Position Graph abstraction can replace the traditional Coupling Graph for LightSABRE-style routing with negligible runtime overhead, showing that a richer architecture model need not come at the cost of slower compilation.
- 4) We provide an open-source implementation of the Position Graph framework and its routing machinery, supporting experimentation across both superconducting and TI-QCCD compilation workflows and future extension across heterogeneous quantum architectures.

II. BACKGROUND

A. Quantum Compilation

In quantum computing, compilation is the process of converting a logical quantum circuit into an equivalent circuit that can be executed directly on a specific quantum processing unit (QPU). This requires adapting the circuit to hardware-dependent constraints, including restricted qudit connectivity, imperfect gate fidelities, and other architectural limitations. Effective compilation is especially important in the NISQ setting, where noise and short coherence times make resource efficiency critical. As a result, quantum compilation generally aims to reduce both circuit size and execution time in order to improve overall reliability. The two central stages of this process are typically (1) transpilation and (2) qudit mapping and routing.

a) Transpilation: The purpose of transpilation is to transform a quantum circuit into an equivalent representation expressed entirely in the native gate set of a target QPU. Because different hardware platforms support different universal gate libraries, this step is necessary to make a circuit physically executable on a given device. For example, superconducting architectures [11] commonly use gates such as SX , RZ ,

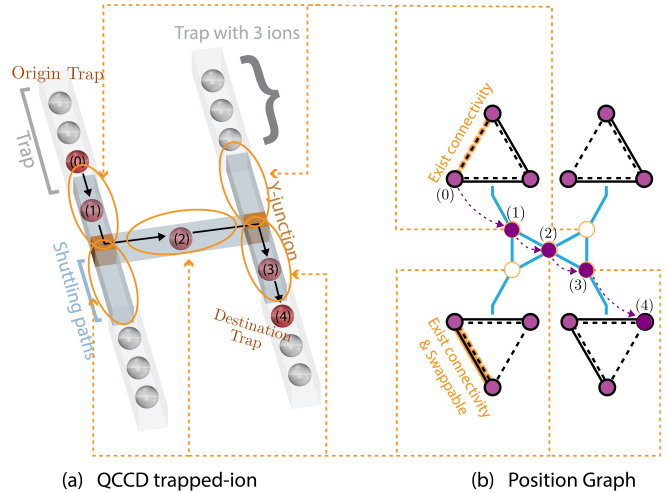


Fig. 1. Example of mapping a QCCD-based TI architecture to its corresponding Position Graph. Figure (a) shows a real hardware configuration, and Figure (b) shows the Position Graph abstraction that represents the hardware configuration. Here, (i) each *position* vertex in the Position Graph represents a physical location where an ion may reside. The vertex colored purple indicates that an ion is currently occupying this location, while the uncolored (white) vertex indicates that this position is empty. (ii) Each vertex with a black border represents the available position inside a trap, while the vertex with a yellow border represents abstract intermediate positions where a qudit may temporarily reside while moving between traps. (iii) The dotted black edges within each trap indicate pairs of positions between which a two-qudit gate operation is possible, while the straight line indicates the physical connection that allows operations such as swap. (iv) The blue edges abstract the path where the ion can move (without stopping) to reach another trap.

and $CNOT$, whereas trapped-ion platforms [12] may instead employ RZ , $U1q$, and RZZ . State-of-the-art methods for transpilation [13] often operate by partitioning a large circuit into smaller subcircuits, computing the unitary implemented by each block, and then re-synthesizing each block in the target native gate set using an appropriate synthesis procedure

b) Qudit Mapping and Routing: Qudit mapping, also referred to as layout, is the compilation stage that assigns the logical qudits of a circuit to the physical qudits of a target architecture while respecting hardware constraints. This problem is most commonly discussed for superconducting platforms, where connectivity is described by a Coupling Graph and multi-qudit gates can only be executed between connected physical qudits. Similar placement requirements also arise in trapped-ion and neutral-atom systems, where each logical qudit must be assigned to a specific ion or atom [1]. Once an initial layout is chosen, qudit routing [14] is used to realize interactions between distant logical qudits by inserting additional operations—typically SWAPs, shuttling operations, or other movement primitives—that bring the relevant qudits into an executable configuration. In superconducting architectures, these routing transitions are typically implemented through SWAP operations between adjacent physical qudits. QCCD-based trapped-ion systems face an analogous routing problem, but the mechanism differs: instead of exchanging logical states through SWAP gates, the compiler coordinates ion shuttling operations that physically move qudits across

the device. Mapping and routing are inherently coupled: the quality of the initial assignment strongly affects the routing overhead, while routing costs in turn influence which assignments are desirable. Because these additional operations can significantly increase circuit depth, gate count, and execution time, mapping and routing are major sources of compilation overhead. Accordingly, modern methods [9], [15]–[18] aim both to find high-quality initial placements and to perform intermediate remapping steps that enable future gates at low cost.

III. RELATED WORK

A. Heuristic Mapping and Routing

Heuristic methods form the dominant practical approach to qudit mapping and routing, primarily because they scale more effectively than exact or solver-based formulations. For superconducting devices, SABRE [9] established the standard heuristic template based on front-layer routing with lookahead. It maintains a front layer of executable gates and an extended lookahead layer, and iteratively inserts SWAPs according to a heuristic that balances immediate and future routing costs; the same procedure can also be applied bidirectionally to obtain improved initial layouts. Recently, PAM [16] extended this framework by combining block-based routing with permutation-aware synthesis, while LightSABRE [17] improved robustness, scalability, and routing quality on larger circuits.

In trapped-ion and especially QCCD architectures, however, heuristic methods must reason not only about logical remapping but also about physical ion transport. Early work therefore emphasized shuttle-aware initial placement and multi-trap compilation, including shuttle-efficient mapping policies and shuttle-reduction heuristics for trapped-ion systems [19], [20]. Recent work has further developed architecture-specific scheduling heuristics for QCCD, including parallel shuttle strategies [21], [22], or adapting the established SABRE method to QCCD architecture through abstraction [8].

B. Analytical Mapping and Routing

In addition to heuristic methods, a substantial line of work has studied qudit mapping and routing through explicit analytical formulations. In superconducting systems, graph-theoretic approaches have modeled the problem using subgraph isomorphism, token swapping, and routing on restricted-connectivity architectures, thereby clarifying its underlying combinatorial structure [2], [23]. Building on this view, several works formulate superconducting mapping and routing as exact optimization problems, including branch-and-bound methods for exact qudit allocation, SMT-based layout synthesis, and integer linear programming models [24]–[26].

Similar analytical directions have recently appeared for trapped-ion architectures. For example, [27] proposes an SMT-based formulation for qudit mapping in one-dimensional trapped-ion systems, whereas [28] formulates exact shuttling in QCCD architectures (considering grid memory zone and single processing zone) as a Boolean satisfiability problem

to minimize the required number of movement timesteps. [8] derived a mixed-integer linear program that fully captures the dynamics of QCCD architecture as described in [19] through their Position Graph abstraction. These approaches are valuable because they yield rigorous optimization baselines and, in some settings, provably optimal schedules, although their runtime usually restricts them to relatively small or moderately sized problem instances. [29].

IV. GROUNDWORK

A. Position Graph Abstraction

We adopt the Position Graph abstraction introduced in [8] as presented in Figure 1. In that work, the abstraction is defined concretely for trapped-ion QCCD architectures. We restate this formulation below and then describe how the abstraction extends to other hardware models.

Definition 1 (Position Graph). *Given a hardware architecture consisting of (1) a set of ion traps T , with $|T| = m$, where each trap $t \in T$ has capacity n_t ions, (2) a set of junctions J , and (3) a set of segments S , we define the Position Graph $G_p = (V, E, \psi)$, where V is the set of vertices, E is the set of edges, and $\psi : E \rightarrow L_E$ is a labeling function that assigns labels to edges from the set L_E .*

A node $i \in V$ corresponds to a possible position of an ion in the device at a given time. An edge $(i, j) \in E$ corresponds to a possible transition of an ion from position $i \in V$ to $j \in V$.

The number of vertices and edges are given by:

$$|V| = \sum_{t \in T} n_t + |S| \quad (1)$$

$$|E| = \sum_{t \in T} (n_t - 1) + \sum_{j \in J} \frac{d(j)(d(j) - 1)}{2} + |J_T| - |J_J|, \quad (2)$$

where j denotes a junction, J_T is the set of segments connecting junctions and traps, J_J is the set of segments connecting pairs of junctions, and $d(j)$ denotes the degree of junction j .

The set of edge labels is defined (for QCCD architectures) as:

$$L_E = \{\text{swap}, \text{merge/split}, \text{move}\}. \quad (3)$$

The swap label corresponds to transitions within a trap, merge/split corresponds to transitions between trap and transport regions, and move corresponds to transitions within transport regions.

While Definition 1 provides a concrete construction for QCCD systems, the Position Graph abstraction itself is more general. At its core, it is a labeled graph $G_p = (V, E, \psi)$ in which vertices represent occupiable physical locations and edges represent valid transitions or interactions between locations. The specific sets T , J , and S define one particular instantiation of this abstraction rather than a requirement of it.

This interpretation enables a unified representation across different hardware architectures. For superconducting systems,

the Position Graph simplifies considerably: each vertex corresponds directly to a physical qudit and is executable, and edges represent allowed two-qudit interactions. In this case, there are no intermediate transport regions (i.e., no junctions or segments), and transitions correspond only to gate execution. Under this specialization, the Position Graph reduces to the well-known Coupling Graph, while preserving the ability to model richer architectural features when needed.

To represent the dynamic state during routing or shuttling, the Position Graph is paired with a placement function

$$\Phi : Q \rightarrow V,$$

which maps each logical qudit in the set Q to a physical position in V . This separation between the static hardware structure (G_p) and the dynamic assignment (Φ) enables efficient reasoning about routing, scheduling, and resource constraints.

B. SHAW: A Shuttling-Aware Heuristic for QCCD Architectures

SHAW (SHuttling-AWAre heuristic) [8] is a SABRE-based routing and mapping algorithm designed for trapped-ion QCCD architectures. Whereas SABRE routes circuits by inserting SWAP operations on a fixed coupling graph, SHAW routes by selecting physically valid ion-shuttling operations on a Position Graph.

In superconducting architectures, a gate is executable when its qudits are adjacent according to the Coupling Graph. In QCCD architectures, a gate is usually executable when the participating ions are co-located within an executable trap. SHAW therefore replaces the SABRE objective of bringing qudits adjacent with the QCCD objective of bringing ions into the same trap.

At a high level, SHAW follows the same iterative structure as SABRE. The algorithm maintains a front layer of gates that are ready to execute. If a front-layer gate is immediately executable, SHAW executes it and advances the frontier. Otherwise, it evaluates candidate shuttling moves and selects the move that minimizes a heuristic cost over the front layer and a small lookahead set.

The cost model reflects the physical constraints of QCCD hardware. Rather than only minimizing graph distance, SHAW evaluates moves according to whether they bring the required ions closer to the same executable trap, reduce the distance among the ions participating in a gate, and respect trap capacity constraints. The Position Graph provides the static hardware structure, while the current ion assignment records, which physical positions are occupied during shuttling.

Thus, SHAW demonstrates that SABRE-based heuristic routing can be extended from static qudit adjacency constraints to dynamic ion placement and trap co-location constraints. The next subsection describes how SHAW handles cases where movement and occupancy constraints create congestion.

C. Congestion Resolution in SHAW

Congestion arises in SHAW when an ion must move along a shuttling path, but an intermediate position on that path is

already occupied. SHAW refers to such an occupied intermediate position as a blockage. When a movement path is blocked, SHAW invokes a congestion-resolution procedure to clear the blockage and allow shuttling to continue.

When congestion resolution is required for a front-layer gate, SHAW first selects an executable target trap for that gate. Candidate traps are evaluated using the estimated cost of moving the gate ions into the trap, together with penalties for congested paths when positions along the required shuttling paths are occupied. Traps with more available space and less congested paths are preferred because they are less likely to introduce additional congestion.

After selecting the target trap, SHAW assigns the participating ions to positions in that trap and attempts to move each ion along a shortest shuttling path. If the next position on the path is unoccupied, the ion moves directly. If the next position is occupied, SHAW attempts to clear the blocking ion.

To clear a blockage, SHAW evaluates nearby positions (except positions on the dedicated path) as possible destinations for the blocking ion. These candidate positions are scored using a local congestion metric: positions whose nearby regions contain fewer occupied positions are preferred. The size of the nearby region is controlled by a search depth. A depth of one considers positions one step away from the candidate position, a depth of two includes positions up to two steps away, and so on. In the implementation used in [8], the initial search depth is one less than the trap capacity, and the depth increases during recursive congestion-resolution calls.

If an available nearby position exists, the blocking ion is moved there; this is called a clearing move. If all nearby positions are themselves occupied, SHAW recursively applies the same procedure to clear one of those secondary blockages. In difficult cases, the resolver may temporarily move the target ion itself to escape a local dead end.

Congestion resolution is therefore a recursive local repair mechanism. It does not change SHAW’s overall SABRE-based search structure; rather, it allows the search to continue when QCCD path, occupancy, and trap-capacity constraints prevent a direct shuttling move.

V. METHODOLOGY

A. Quantum Architecture Caching

Most qudit routing and mapping algorithms across different architectures can use the Position Graph as the central architecture representation. Since the architecture does not change during a compilation run, architecture-dependent quantities can be computed once and reused throughout routing. These quantities include an all-pairs distance matrix for the positions in the Position Graph and the corresponding shortest paths list. Using the Position Graph’s edge labels and selecting the edges annotated with execute functionality, we can derive and cache an execution subgraph from the original Position Graph. This execution subgraph is used for efficiently determining whether a multi-qudit gate can be performed.

In our implementation, this design exposed repeated computations in both BQSKit’s SABRE implementation [10] and

the original SHAW implementation [8], including repeated distance and path calculations, and repeated checks on allowed gate execution. Moving these architecture-level queries into Position Graph caches reduced this overhead without changing the routing decisions. The remainder of this section focuses on the additional caching introduced for the implementation of the SHAW algorithm, which we will refer to as LightSHAW from here on. LightSHAW also introduces a SHAW-specific global cache of path blockage profiles and local caches that help make SHAW’s congestion resolution more efficient. These caches are specific to the TI-QCCD architecture.

B. LightSHAW Global Path Blockage Profiles

In our LightSHAW implementation, we introduce a new global cache of path blockage profiles for each source-target movement path. A path blockage profile is the list of intermediate positions along a selected movement path that could block the move if occupied, together with the fixed penalty associated with resolving a blockage at each such position.

For a movement from position s to position t , the profile depends only on the Position Graph and on the fixed costs assigned to physical shuttling operations. It does not depend on the current ion assignment. During scoring, LightSHAW checks the current assignment only to determine which positions in the profile are occupied.

This cache is useful because SHAW repeatedly scores candidate moves between the same pairs of positions. By caching the path and the fixed blockage penalties, LightSHAW avoids reconstructing the same path and recomputing the same static penalty terms on each scoring call. The cached profile does not determine that a path is blocked; it only provides the reusable list of positions that must be checked against the current ion assignment.

C. LightSHAW Congestion Memoization

Architecture-level caches are insufficient for congestion resolution because congestion depends on the current ion assignment. When SHAW attempts to clear a blocked movement path, it evaluates candidate clearing positions among the blocking ions by examining which nearby positions are currently occupied. These local congestion evaluations can recur during recursive clearing.

LightSHAW preserves the congestion-resolution logic of SHAW but avoids recomputing repeated local evaluations. It implements this optimization as a two-level cache. The first level caches the local scoring set: for a given candidate clearing position, it stores the positions that should be inspected when computing congestion. The second level memoizes the resulting congestion score for the current occupancy of that local scoring set.

a) Local Scoring-Set Cache: During recursive congestion resolution, SHAW repeatedly evaluates nearby locations as possible destinations for a blocking ion. For each candidate clearing position p , target position t , blockage position b , and search depth d , LightSHAW builds the local scoring set:

$$\mathcal{N}_d(p, t, b).$$

This set contains positions reachable from p within d movement steps, excluding the blockage position b and the local target position t for the current clearing move. These exclusions keep the scoring region focused on places where the blocking ion could be moved without immediately undoing the clearing move. This set is then cached and does not decide which candidate position should be used. Instead, for each candidate position already being considered by SHAW, it answers the question: which positions should be inspected when scoring this candidate move? LightSHAW caches this set under the tuple (p, t, b, d) and reuses it whenever the same local structure is evaluated again.

b) Configuration-Keyed Congestion Memoization: After retrieving the local scoring set: $\mathcal{N}_d(p, t, b)$ either from cache or by constructing the first time, LightSHAW checks which positions in that set are currently occupied. It does not store the full ion assignment in the cache key. Instead, it forms a *local occupancy signature* σ , which records only the occupied positions among the candidate position p and the positions in $\mathcal{N}_d(p, t, b)$.

For example, suppose SHAW is evaluating candidate position $p = 3$, and the cached local scoring set is

$$\mathcal{N}_d(3, t, b) = \{4, 5, 7, 9\}.$$

If positions 5 and 9 are occupied, while positions 3, 4, and 7 are empty, then

$$\sigma = (5, 9).$$

If position 3 were also occupied, then

$$\sigma = (3, 5, 9).$$

Ions outside the candidate position and its local scoring set are not included because they do not affect the congestion score for this candidate move.

The congestion score is memoized using the key

$$(p, t, b, d, \sigma).$$

On a cache miss, LightSHAW computes the same congestion quantities used by SHAW: the fraction of occupied positions in the local scoring set and a weighted score that gives greater importance to occupied positions closer to the candidate location. On a cache hit, the stored result is reused.

Because the key includes σ , the cached value remains valid even if ions outside the local scoring set move. If the occupancy of the local scoring set changes, then σ changes, and the score is recomputed. The cache is scoped to a single congestion-resolution episode and is passed through the recursive calls generated while clearing a blocked movement path. This captures repeated local states during recursive clearing without allowing the cache to grow across the entire compilation. Together, these two caches preserve SHAW’s congestion decisions while reducing the repeated graph traversal and local occupancy scanning needed to score candidate clearing moves.

D. Pruning Trap Selection

During brute-force or congestion resolution, when a multi-qudit operation cannot be executed and gets stuck at the current ion assignment, the mapper must choose a candidate trap where the participating ions should be moved. An exhaustive implementation scores every executable trap exactly, but this is expensive because the exact score considers distinct assignments of ions to trap slots and includes congestion-resolution penalties along the selected paths, especially when the number of considered traps scales. We reduce this cost by first computing lower-bound scores for all traps. These traps are then evaluated as candidates in lower-bound score order, and exact scoring stops once no remaining lower bound can improve on the best exact score found so far.

In more detail, for each trap, we compute an optimistic lower bound on the cost of routing the participating ions into that trap. For each position in the position graph and each trap, we cache the shortest travel distance from that position to the closest position within the trap. The found score is the sum of these nearest-trap distances over the participating ions' current positions. This bound ignores congestion and the requirement that different ions occupy distinct trap positions.

Each trap's score is then adjusted by its current occupancy: traps with more available positions receive a small bonus. Because the same adjustment is applied to both the lower bound and the exact score, the adjusted lower bound can only underestimate or equal the corresponding adjusted exact score.

Candidate traps are sorted by this lower bound. We then evaluate traps in that order using the exact scoring routine. Exact scoring considers the same shortest-path distances, but also adds congestion-resolution penalties for occupied positions along the paths. The exact scorer also enforces that each participating ion is assigned to a distinct position within the candidate trap.

As exact scores are computed, we maintain the best exact score found so far. Once the next candidate trap's lower bound is greater than the current best exact score, that trap cannot improve the solution. Since the candidate list is sorted by increasing lower bound, all remaining traps cannot improve the solution and are pruned without exact scoring.

E. Discussion on memory usage for memoization

The caching strategies described above trade memory for reduced repeated computation. Let $|V|$ denote the number of positions in the Position Graph, $|T|$ denote the number of executable traps, and $\text{diam}(G_p)$ denote the diameter of the position graph

The all-pairs distance matrix requires $O(|V|^2)$ memory. The shortest path list has the worst-case memory as $O(|V|^2 \text{diam}(G_p))$, since each source-target pair may store a path whose length grows with the architecture diameter.

The path blockage profile cache stores, for queried source-target movement pairs, the intermediate positions along the path, and the fixed blockage resolution cost for each such position. In the worst case, if every pair of positions are queried, this cache also has the memory of $O(|V|^2 \text{diam}(G_p))$.

In practice, the actually memorys can grow much slower as it only considers the number of shuttling paths actually scored during compilation.

The trap-pruning cache stores the nearest distance from each position in the Position Graph to each executable trap. Its memory requirement is $O(|V||T|)$.

For a k -qudit operation, the lower-bound score for a trap is computed on demand by summing k entries from this cache. We intentionally avoid caching the combined lower-bound score for tuples of participating ion positions, because such a cache would scale as $O(|V|^k|T|)$, which becomes prohibitive for large architectures.

Congestion memoization has two memory components. The geometry-only local scoring-set cache stores neighborhoods of the form $\mathcal{N}_d(p, t, b)$, and scales with the number of unique local congestion geometries encountered:

$$O(NL),$$

where N is the number of cached (p, t, b, d) tuples and L is the average size of the corresponding local scoring set. The occupancy-dependent congestion score cache is scoped to a single congestion-resolution episode. Its memory scales with the number of distinct local occupancy signatures encountered during that episode and is discarded afterward.

These caches reduce repeated graph traversal, path reconstruction, and local occupancy scoring. Their drawback is that the geometry-dependent caches can grow substantially as the architecture size increases, especially caches with quadratic dependence on $|V|$. For this reason, LightSHAW caches reusable single-position and single-path quantities, but avoids caching combined multi-ion trap scores whose key space grows combinatorially.

VI. EXPERIMENTS

A. Experimental setup

Our experiments use a diverse benchmark suite consisting of well-known quantum algorithms and Hamiltonian simulation circuits with sizes ranging from 16 to 512 qudits. The suite includes the Quantum Approximate Optimization Algorithm (QAOA) [30], the Quantum Fourier Transform (QFT) [31], and Hamiltonian simulation circuits for the Transverse Field Ising Model (TFIM) and Transverse Field XY (TFXY) model. QAOA is a variational algorithm for combinatorial optimization and is widely used as a representative NISQ workload. QFT is a core algorithmic primitive used in larger quantum algorithms, including Quantum Phase Estimation [32] and Shor's factoring algorithm [33]. TFIM and TFX Y represent structured Hamiltonian simulation workloads, which are central to many near-term quantum computing applications.

The QFT and QAOA circuits are generated using Qiskit [34]. For QAOA, we construct instances from Erdős-Rényi graphs with edge probability $p = 0.1$. The TFIM and TFX Y circuits are generated using the F3C++ compiler [35].

To isolate the effect of the proposed Position Graph abstraction, we first compare LightSABRE [17] using the conventional coupling-graph representation against LightSABRE

using our Position Graph abstraction. We then evaluate SHAW [8] and LightSHAW, as described in the methodology, to study the impact of architecture caching and congestion memoization in the shuttling-based setting. Together, these experiments serve as an ablation study that separates the contributions of the Position Graph abstraction from those of the LightSHAW memoization strategy.

We implement the Position Graph abstraction in Python 3.11 as an extension to BQSKit [10]. We evaluate the scalability of LightSHAW against SHAW and QCCDSim [19], a state-of-the-art QCCD shuttling simulator. All experiments are performed on a Gen3 Intel Xeon Gold 6240R system with 1 TB of main memory. Since QCCDSim only supports circuits transpiled to a gate set containing CNOT gates, we first transpile all input circuits to the required gate set using BQSKit to enable a fair comparison.

Reproducibility: Our source code and results are available at [link will be added here upon acceptance].

B. Experimental results

a) *QCCD Compilation time comparison:* We first evaluate the impact of the proposed caching techniques by comparing LightSHAW, SHAW, and QCCDSim compilation times through Figure 2. Our results show that LightSHAW significantly reduces compilation time from SHAW by eliminating redundant recomputation during shuttling. The LightSHAW compilation time results are more comparable to QCCDSim. LightSHAW presently takes additional time for shorter circuits, but when considering circuits on 180-ion architecture, we start to match and outperform QCCDSim compilation runtime. Furthermore, the results show better compilation time scaling compared to SHAW when performing power law fitting model $y = ax^b$, where x is the total number of qubits. For small to medium-sized benchmark (less than 100-qubit circuits), QCCDSim consistently achieves lower compilation time, whereas LightSHAW takes longer compilation time due to additional overhead from its generalized abstraction and congestion-aware heuristic search. Despite this overhead, LightSHAW always has better performance, as shown in Table I, and still shows a compilation time scaling advantage when comparing with QCCDSim, where we can see that the exponent factor b for LightSHAW is around 1.72, which is much better than QCCDSim, around 3.04.

Besides considering the compilation time, Operation time (gate execution time and shuttling time) is a critical factor for near-term Trapped-Ion quantum devices. Following the gate fidelity model described in [19], longer operation times increase gate noise, which directly degrades circuit fidelity. Prior work has shown that reducing operation time is essential for improving reliability on noisy hardware [4], [19]. We evaluate the quality of the resulting LightSHAW and QCCDSim compilations in terms of operation time in Table I.

Table I shows total operation time across different benchmarks with different architectures. As shown, LightSHAW consistently produces a schedule with much lower operation time compared to QCCDSim. This suggests that the caching

TABLE I
TOTAL OPERATION TIME COMPARISON FOR LIGHTSHAW AND QCCDSIM ON GRID ARCHITECTURES. LOWER VALUES CORRESPOND TO SHORTER EXECUTION TIME + SHUTTLING TIME AND IMPROVED CIRCUIT EFFICIENCY.

Benchmark	Arch	Ions/Trap	LightSHAW (μ s)	QCCDSim (μ s)	Ratio
QAOA_16	2 × 2	5	21091	39680	0.532
QFT_16	2 × 2	5	25327	53880	0.470
TFIM_16	2 × 2	5	15603	39260	0.397
TFXY_16	2 × 2	5	19171	29980	0.639
QAOA_32	3 × 3	5	45385	77100	0.589
QFT_32	3 × 3	5	123523	193360	0.639
TFIM_32	3 × 3	5	150577	182300	0.826
TFXY_32	3 × 3	5	148751	160920	0.924
QAOA_64	4 × 4	5	102357	158260	0.647
QFT_64	4 × 4	5	323839	629820	0.514
TFIM_64	4 × 4	5	692951	1193240	0.581
TFXY_64	4 × 4	5	680465	1094320	0.622
QAOA_128	6 × 6	5	432382	908440	0.476
QFT_128	6 × 6	5	616460	1493960	0.413
TFIM_128	6 × 6	5	3271462	3762880	0.869
TFXY_128	6 × 6	5	3271462	3762880	0.869
QAOA_256	8 × 8	5	1872099	5450600	0.343
QFT_256	8 × 8	5	1736270	5171360	0.336
QAOA_512	10 × 10	6	4705827	27545320	0.171
QFT_512	10 × 10	6	1960315	9972900	0.197
QAOA_1024	13 × 13	8	3525259	148271360	0.024
QFT_1024	13 × 13	8	4492742	21024420	0.213

strategy not only allows LightSHAW to have a better compilation time scaling than QCCDSim but also maintains the operation time improvement from the original SHAW.

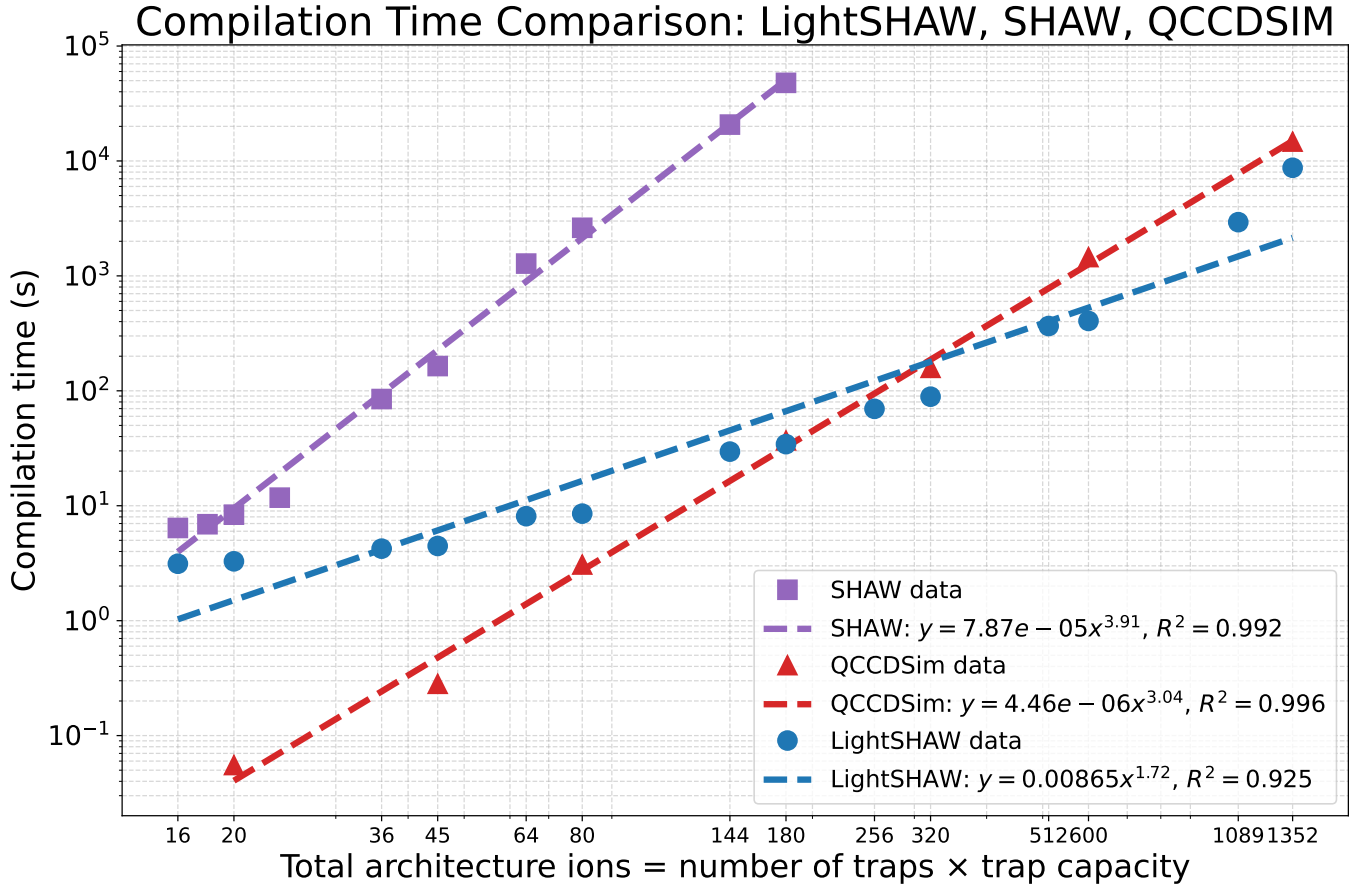


Fig. 2. Average compilation time (s) of SHAW, LightSHAW, and QCCDSim across multiple benchmark circuits at different circuit sizes and architectures. The figure is shown on a logarithmic scale. The data point shows average compile times at a given architecture ($\text{Grid}x \times y$ with k ions per trap). The dashed curves show power-law fits of the form $y = ax^b$, where x is the total number of ions inside the architectures (total number of traps \times Trap capacity). Both SHAW and LightSHAW can solve stricter architectures than QCCDSim, as shown in Table III, which results in more data points than QCCDSim. The fitted exponents indicate the observed growth rates: SHAW scales approximately as $x^{3.91}$, LightSHAW as $x^{1.72}$, and QCCDSim as $x^{3.04}$.

Beyond improved performance, similar to SHAW, LightSHAW demonstrates significantly improved robustness. As shown in Table II, QCCDSim fails to produce valid compilations for all the strict architectures where the congestion is high (denoted by X). In contrast, LightSHAW consistently produces valid compilations for these examples and can do so across a broader range of circuits and architectures. This indicates that LightSHAW can significantly improve the practical executability of quantum circuits on noisy hardware.

Overall, these results show that QCCDSim remains faster for small to medium instances where it successfully solves. On the other hand, LightSHAW provides a compilation approach capable of handling a wider range of circuits while maintaining practical compilation time, and even better for big instances, producing schedules with much better operation time.

b) Compatibility of Coupling Graph and Position Graph shown on LightSABRE: To evaluate the overhead of the Position Graph abstraction in a setting where a traditional Coupling Graph is sufficient, we implemented LightSABRE using both abstractions. The Coupling Graph backend serves

as the standard superconducting-device baseline, representing the architecture through physical adjacency and distance. The Position Graph backend uses a similar logic, but stores architecture information in a richer labeled graph.

At the time of testing, BQSKit’s SABRE algorithm did not have the relative scoring described by LightSABRE implemented. To enable better scaling and experiments with larger circuits, we implemented the relative scoring technique with both the Coupling Graph and Position Graph implementations. We were able to implement the Position Graph such that the same SWAP operations are chosen as the version featuring the Coupling Graph. This allows for a more direct measurement of the overhead of the Position Graph.

Profiling revealed two architecture-level queries that were repeatedly computed in the Coupling Graph implementation. First, the original executability check validated multi-qudit gates by constructing an induced subgraph and checking whether it was connected. Although a single subgraph construction is inexpensive, this check is called millions of times on larger circuits. Table III shows the impact of replacing

TABLE II

OPERATION TIME RESULTS FOR ARCHITECTURES WITH A STRICTER NUMBER OF IONS PER TRAP (HIGHER ION UTILIZATION). QCCDSIM FAILS TO PRODUCE VALID COMPILATIONS (DENOTED BY X), WHILE LIGHTSHAW SUCCESSFULLY COMPLETES ALL INSTANCES, DEMONSTRATING IMPROVED ROBUSTNESS UNDER TIGHTER RESOURCE CONSTRAINTS.

Benchmark	Arch	Ions/Trap	LightSHAW (μ s)	QCCDSim (μ s)
QAOA_16	2×2	4	29166	X
QFT_16	2×2	4	34345	X
TFIM_16	2×2	4	27727	X
TFXY_16	2×2	4	28814	X
QAOA_32	3×3	4	50118	X
QFT_32	3×3	4	143611	X
TFIM_32	3×3	4	173341	X
TFXY_32	3×3	4	167387	X
QAOA_64	4×4	4	105128	X
QFT_64	4×4	4	335942	X
TFIM_64	4×4	4	790249	X
TFXY_64	4×4	4	777260	X
QAOA_128	6×6	4	444328	X
QFT_128	6×6	4	616460	X
TFIM_128	6×6	4	3271462	X
TFXY_128	6×6	4	3391871	X
QAOA_256	8×8	4	1150680	X
QFT_256	8×8	4	1285258	X
QAOA_512	8×8	8	4647942	X
QFT_512	8×8	8	1639341	X
QAOA_1024	11×11	9	18817281	X
QFT_1024	11×11	9	3408264	X

repeated subgraph construction with the same information cached by the Position Graph.

Second, the Coupling Graph implementation recomputed all-pairs shortest paths at the beginning of each forward and backward SABRE pass. With two layout passes and the routing pass this results in five all-pairs computations. On the 512-qudit benchmarks, each call takes roughly 40 seconds. In contrast, the Position Graph stores the corresponding path and distance information with the architecture object and reuses it across passes. Table IV shows this profiling difference.

These optimizations are not inherently exclusive to the Position Graph; similar caches can also be added to a Coupling Graph implementation. The significance of the result is that the Position Graph exposes these architecture-level queries as part of the graph representation. As shown in Figure 3, when both back ends use comparable caching and relative scoring, the position graph matches the compilation time of the Coupling Graph with negligible overhead while preserving the ability to represent more types of architectures. This supports the Position Graph as a practical common representation for both SWAP-based superconducting routing and shuttling-based QCCD routing.

These results show that the Position Graph can replace the Coupling Graph for SABRE-based routing without introducing meaningful overhead. When the target architecture is simple, the Position Graph behaves like a Coupling Graph. When the architecture is richer, the same object can expose movement paths, execution regions, edge capabilities, and weighted costs. This allows a single architecture representation to support both

standard SABRE/LightSABRE for superconducting systems and SHAW/LightSHAW for more complex TI-QCCD systems.

VII. DISCUSSION

A central implication of these results is that richer architecture representations need not impose a prohibitive runtime cost. In the superconducting-style LightSABRE experiments, the Position Graph matched the behavior and runtime of a coupling-graph implementation while retaining additional structure needed for QCCD routing. This suggests that compiler infrastructure can move beyond minimal adjacency models without necessarily sacrificing scalability.

Many routing workflows represent hardware connectivity primarily as a binary relation: two qudits either can interact directly, or they cannot. In practice, operations are not equally desirable across all physical locations or interactions. Real devices exhibit heterogeneity in gate duration, error rate, movement cost, and reliability. The Position Graph provides a natural interface for representing this heterogeneity through edge and position labels, weights, and capabilities. In this work, these quantities are treated as static during compilation. A natural extension is to update them dynamically from calibration data or time-varying device conditions, allowing routing decisions to adapt without changing the underlying architecture abstraction.

The same abstraction can also represent operations beyond local movement or nearest-neighbor gates. For example, teleportation-based interactions, long-range entanglement links, or photonic interconnects could be modeled as additional edge capabilities with distinct costs and constraints. Similarly, frequently occurring multi-step procedures could be represented as composite actions with precomputed costs. This would allow a routing algorithm to evaluate higher-level transformations alongside primitive operations such as swaps, moves, splits, and merges.

ACKNOWLEDGMENT

This work was supported in part by NSF award #2444042.

REFERENCES

- [1] Chenghong Zhu, Xian Wu, Zhaohui Yang, Jingbo Wang, Anbang Wu, Shenggen Zheng, and Xin Wang. Quantum compiler design for qubit mapping and routing: A cross-architectural survey of superconducting, trapped-ion, and neutral atom systems. *arXiv preprint arXiv:2505.16891*, 2025.
- [2] Alexander Cowtan, Silas Dilkes, Ross Duncan, Alexandre Krajenbrink, Will Simmons, and Seyon Sivarajah. On the qubit routing problem. *arXiv preprint arXiv:1902.08091*, 2019.
- [3] Wen Ning, Xin-Jie Huang, Pei-Rong Han, Hekang Li, Hui Deng, Zhen-Biao Yang, Zhi-Rong Zhong, Yan Xia, Kai Xu, Dongning Zheng, et al. Deterministic entanglement swapping in a superconducting circuit. *Physical review letters*, 123(6):060502, 2019.
- [4] M Malinowski, DTC Allcock, and CJ Ballance. How to wire a 1000-qubit trapped-ion quantum computer. *PRX Quantum*, 4(4):040313, 2023.
- [5] Juan M Pino, Jennifer M Dreiling, Caroline Figgatt, John P Gaebler, Steven A Moses, MS Allman, CH Baldwin, Michael Foss-Feig, David Hayes, Karl Mayer, et al. Demonstration of the trapped-ion quantum ccd computer architecture. *Nature*, 592(7853):209–213, 2021.
- [6] Adam Siegel, Armands Strikis, and Michael Fogarty. Towards early fault tolerance on a $2 \times n$ array of qubits equipped with shuttling. *PRX Quantum*, 5(4):040328, 2024.

TABLE III
 PROFILING OF `_can_exe` IMPLEMENTATIONS IN LIGHTSABRE. CG EVALUATES EXECUTABILITY USING REPEATED SUBGRAPH EXTRACTION, WHEREAS PG USES CACHED POSITION GRAPH EXECUTE ADJACENCY. VALUES ARE AVERAGED OVER TWO RUNS.

Benchmark	Method	Total (s)	<code>_can_exe</code> (s)	# Calls	<code>get_subgraph</code> (s)
QAOA_128	CG	41.69	14.06	254445	11.38
QAOA_128	PG	28.84	2.13	254445	–
QFT_128	CG	21.69	5.75	93206	4.69
QFT_128	PG	14.06	0.84	93206	–
QAOA_256	CG	318.57	111.27	1914174	89.98
QAOA_256	PG	220.89	16.90	1914174	–
QFT_256	CG	95.26	24.82	403538	20.17
QFT_256	PG	51.92	3.49	403538	–
QAOA_512	CG	2375.96	816.92	11786673	659.05
QAOA_512	PG	1508.63	115.23	11786673	–
QFT_512	CG	447.85	80.09	1149807	64.83
QFT_512	PG	193.94	11.51	1149807	–

LightSABRE Compilation Time: Coupling Graph vs Position Graph

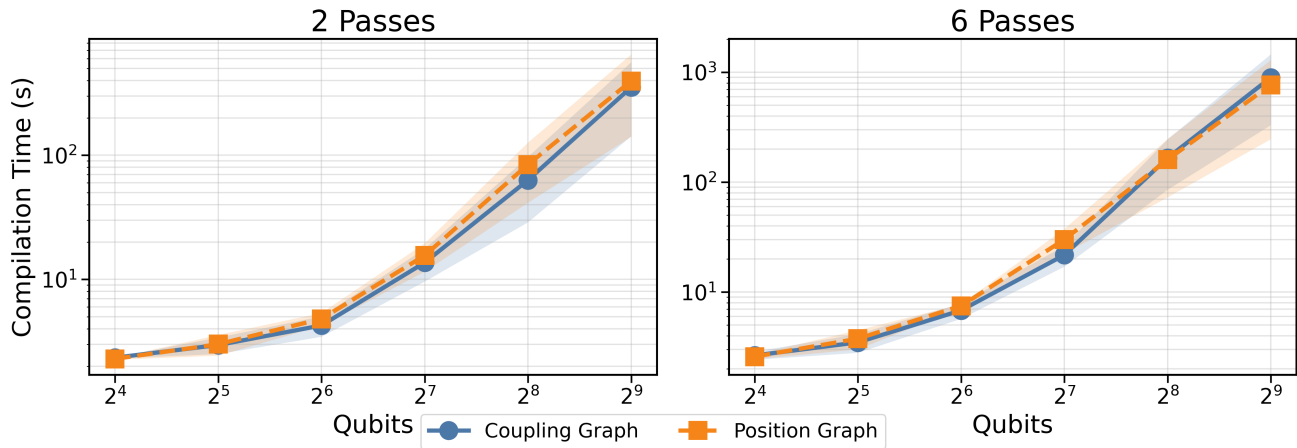


Fig. 3. LightSABRE compilation time comparing Coupling Graph and Position Graph representations across QFT and QAOA benchmarks with varying qudit counts and 2 or 6 layout passes. This data includes caching strategies added to the Coupling Graph implementation. Results are shown on a logarithmic scale. Both representations produce identical compiled circuits, allowing a direct comparison of compilation time.

TABLE IV
 ALL-PAIRS SHORTEST-PATH PROFILING COMPARISON BETWEEN COUPLING GRAPH (CG) AND POSITION GRAPH (PG) REPRESENTATIONS IN 512-QUDIT LIGHTSABRE RUNS. THE POSITION GRAPH PERFORMS A SINGLE PRECOMPUTATION, WHEREAS THE COUPLING GRAPH RECOMPUTES SHORTEST PATHS MULTIPLE TIMES. RESULTS ARE AVERAGED OVER TWO RUNS WITH 2 LAYOUT PASSES.

Benchmark	Method	Calls	Cum. Time (s)	Total (s)
QAOA_512	CG	5	210.62	2375.96
QAOA_512	PG	1	26.49	1508.63
QFT_512	CG	5	202.03	447.85
QFT_512	PG	1	27.17	193.94

[7] Maxim De Smet, Yuta Matsumoto, Anne-Marije J Zwerver, Larysa Tryputen, Sander L de Snoo, Sergey V Amitonov, Sam R Katirae-Far, Amir Sammak, Nodar Samkharadze, Önder Gül, et al. High-fidelity single-spin shuttling in silicon. *Nature Nanotechnology*, 20(7):866–872, 2025.

[8] Bao Bach, Ilya Safro, and Ed Younis. Efficient compilation for shuttling trapped-ion machines via the position graph architectural abstraction.

arXiv preprint arXiv:2501.12470, 2025.

[9] Gushu Li, Yufei Ding, and Yuan Xie. Tackling the qubit mapping problem for nisq-era quantum devices. In *Proceedings of the twenty-fourth international conference on architectural support for programming languages and operating systems*, pages 1001–1014, 2019.

[10] Ed Younis, Costin C Iancu, Wim Lavrijsen, Marc Davis, and Ethan Smith. Berkeley quantum synthesis toolkit (bqskit) v1. Technical report, Lawrence Berkeley National Laboratory (LBNL), Berkeley, CA (United States), 2021.

[11] Jens Koch, Terri M Yu, Jay Gambetta, Andrew A Houck, David I Schuster, Johannes Majer, Alexandre Blais, Michel H Devoret, Steven M Girvin, and Robert J Schoelkopf. Charge-insensitive qubit design derived from the cooper pair box. *Physical Review A—Atomic, Molecular, and Optical Physics*, 76(4):042319, 2007.

[12] David Kielpinski, Chris Monroe, and David J Wineland. Architecture for a large-scale ion-trap quantum computer. *Nature*, 417(6890):709–711, 2002.

[13] Ed Younis and Costin Iancu. Quantum circuit optimization and transpilation via parameterized circuit instantiation. In *2022 IEEE International Conference on Quantum Computing and Engineering (QCE)*, pages 465–475. IEEE, 2022.

[14] Aniruddha Bapat, Andrew M Childs, Alexey V Gorshkov, and Eddie Schoute. Advantages and limitations of quantum routing. *PRX quantum*, 4(1):010313, 2023.

- [15] Debjyoti Bhattacharjee, Abdullah Ash Saki, Mahabubul Alam, Anupam Chattopadhyay, and Swaroop Ghosh. Muqut: Multi-constraint quantum circuit mapping on nisq computers. In *2019 IEEE/ACM international conference on computer-aided design (ICCAD)*, pages 1–7. IEEE, 2019.
- [16] Ji Liu, Ed Younis, Mathias Weiden, Paul Hovland, John Kubiatowicz, and Costin Iancu. Tackling the qubit mapping problem with permutation-aware synthesis. In *2023 IEEE International Conference on Quantum Computing and Engineering (QCE)*, volume 1, pages 745–756. IEEE, 2023.
- [17] Henry Zou, Matthew Treinish, Kevin Hartman, Alexander Ivrii, and Jake Lishman. Lightsabre: A lightweight and enhanced sabre algorithm. *arXiv preprint arXiv:2409.08368*, 2024.
- [18] Ge Yan, Wenjie Wu, Yuheng Chen, Kaisen Pan, Xudong Lu, Zixiang Zhou, Yuhan Wang, Ruocheng Wang, and Junchi Yan. Quantum circuit synthesis and compilation optimization: Overview and prospects. *arXiv preprint arXiv:2407.00736*, 2024.
- [19] Prakash Murali, Dripto M Debroy, Kenneth R Brown, and Margaret Martonosi. Architecting noisy intermediate-scale trapped ion quantum computers. In *2020 ACM/IEEE 47th Annual International Symposium on Computer Architecture (ISCA)*, pages 529–542. IEEE, 2020.
- [20] Abdullah Ash Saki, Rasit Onur Topaloglu, and Swaroop Ghosh. Muzzle the shuttle: Efficient compilation for multi-trap trapped-ion quantum computers. In *2022 Design, Automation & Test in Europe Conference & Exhibition (DATE)*, pages 322–327. IEEE, 2022.
- [21] Chenghong Zhu, Xian Wu, Jingbo Wang, and Xin Wang. S-sync: Shuttle and swap co-optimization in quantum charge-coupled devices. In *Proceedings of the 52nd Annual International Symposium on Computer Architecture*, pages 271–284, 2025.
- [22] Jixuan Ruan, Hezi Zhang, Xiang Fang, Ang Li, Wesley C Campbell, Eric Hudson, David Hayes, Hartmut Haeffner, Travis Humble, Jens Palsberg, et al. Trapsimd: Simd-aware compiler optimization for 2d trapped-ion quantum machines. *arXiv preprint arXiv:2504.17886*, 2025.
- [23] Marcos Yukio Siraichi, Vinícius Fernandes dos Santos, Caroline Colange, and Fernando Magno Quintão Pereira. Qubit allocation as a combination of subgraph isomorphism and token swapping. *Proceedings of the ACM on Programming Languages*, 3(OOPSLA):1–29, 2019.
- [24] Pengcheng Zhu, Xueyun Cheng, and Zhijin Guan. An exact qubit allocation approach for nisq architectures. *Quantum Information Processing*, 19(11):391, 2020.
- [25] Bochen Tan and Jason Cong. Optimal layout synthesis for quantum computing. In *Proceedings of the 39th International Conference on Computer-Aided Design*, pages 1–9, 2020.
- [26] Giacomo Nannicini, Lev S Bishop, Oktay Günlük, and Petar Jurcevic. Optimal qubit assignment and routing via integer programming. *ACM Transactions on Quantum Computing*, 4(1):1–31, 2022.
- [27] Wei-Hsiang Tseng, Yao-Wen Chang, and Jie-Hong Roland Jiang. Satisfiability modulo theories-based qubit mapping for trapped-ion quantum computing systems. In *Proceedings of the 2024 International Symposium on Physical Design*, pages 245–253, 2024.
- [28] Daniel Schoenberger, Stefan Hillmich, Matthias Brandl, and Robert Wille. Using boolean satisfiability for exact shuttling in trapped-ion quantum computers. In *2024 29th Asia and South Pacific Design Automation Conference (ASP-DAC)*, pages 127–133. IEEE, 2024.
- [29] Chi Zhang, Ari B Hayes, Longfei Qiu, Yuwei Jin, Yanhao Chen, and Eddy Z Zhang. Time-optimal qubit mapping. In *Proceedings of the 26th ACM international conference on architectural support for programming languages and operating systems*, pages 360–374, 2021.
- [30] Edward Farhi, Jeffrey Goldstone, and Sam Gutmann. A quantum approximate optimization algorithm. *arXiv preprint arXiv:1411.4028*, 2014.
- [31] Michael A Nielsen and Isaac L Chuang. *Quantum computation and quantum information*, volume 2. Cambridge university press Cambridge, 2001.
- [32] Daniel S Abrams and Seth Lloyd. Quantum algorithm providing exponential speed increase for finding eigenvalues and eigenvectors. *Physical Review Letters*, 83(24):5162, 1999.
- [33] Peter W Shor. Polynomial-time algorithms for prime factorization and discrete logarithms on a quantum computer. *SIAM review*, 41(2):303–332, 1999.
- [34] Ali Javadi-Abhari, Matthew Treinish, Kevin Krsulich, Christopher J. Wood, Jake Lishman, Julien Gacon, Simon Martiel, Paul D. Nation, Lev S. Bishop, Andrew W. Cross, Blake R. Johnson, and Jay M. Gambetta. Quantum computing with Qiskit, 2024.
- [35] Efehan Kökcü, Daan Camps, Lindsay Bassman Ofetlie, James K Fredericks, Wibe A de Jong, Roel Van Beeumen, and Alexander F Kemper. Algebraic compression of quantum circuits for hamiltonian evolution. *Physical Review A*, 105(3):032420, 2022.